

# Thermodynamics of the $S = 1/2$ hyperkagome-lattice Heisenberg antiferromagnet

Taras Hutak,<sup>1</sup> Taras Krokhmalskii,<sup>1</sup> Oleg Derzhko,<sup>1,2,3</sup> Jürgen Schnack,<sup>3</sup> and Johannes Richter<sup>4,5</sup>

<sup>1</sup>*Institute for Condensed Matter Physics, National Academy of Sciences of Ukraine, Svientsitskii Street 1, 79011 L'viv, Ukraine*

<sup>2</sup>*Professor Ivan Vakarchuk Department for Theoretical Physics,*

*Ivan Franko National University of L'viv, Drahomanov Street 12, 79005 L'viv, Ukraine*

<sup>3</sup>*Fakultät für Physik, Universität Bielefeld, Postfach 100131, 33501 Bielefeld, Germany*

<sup>4</sup>*Institut für Physik, Otto-von-Guericke-Universität Magdeburg, P.O. Box 4120, 39016 Magdeburg, Germany*

<sup>5</sup>*Max-Planck-Institut für Physik komplexer Systeme, Nöthnitzer Straße 38, 01187 Dresden, Germany*

(Dated: November 15, 2023)

The  $S = 1/2$  hyperkagome-lattice Heisenberg antiferromagnet, which for instance is related to the experimentally accessible spinel oxide  $\text{Na}_4\text{Ir}_3\text{O}_8$ , allows to study the interplay of geometrical frustration and quantum as well as thermal fluctuations in three dimensions. We use 16 terms of a high-temperature series expansion complemented by the entropy-method interpolation to examine the specific heat and the uniform susceptibility of the  $S = 1/2$  hyperkagome-lattice Heisenberg antiferromagnet. We obtain thermodynamic quantities for the two possible scenarios of either a gapless or a gapped energy spectrum. We have found that the specific heat  $c$  exhibits, besides the high-temperature peak around  $T \approx 0.669$ , a low-temperature one at  $T \approx 0.021 \dots 0.033$ . The functional form of the uniform susceptibility  $\chi$  below about  $T = 0.5$  depends strongly on whether the energy spectrum is gapless or gapped. The value of the ground-state energy can be estimated to  $e_0 \approx -0.440 \dots -0.435$ . In addition to the entropy-method interpolation we use the finite-temperature Lanczos method to calculate  $c$  and  $\chi$  for finite lattices of  $N = 24$  and  $36$  sites. A combined view on both methods leads us to favour a gapless scenario since then the maximum of the susceptibility agrees better between both methods.

## I. INTRODUCTION

Frustrated quantum spin systems are a subject of intense ongoing research in the field of magnetism [1–4]. Geometric frustration and quantum fluctuations may evade any ground-state ordering even in three dimensions. Among several famous examples, the  $S = 1/2$  pyrochlore-lattice Heisenberg antiferromagnet has attracted much attention, being for decades a candidate for the realization of a spin-liquid state in three dimensions [5]. After intense numerical studies, a lattice symmetry breaking in the ground state has been revealed [6–9].

A closely related example is the  $S = 1/2$  hyperkagome-lattice Heisenberg antiferromagnet. Inspired by experiments on the spinel oxide  $\text{Na}_4\text{Ir}_3\text{O}_8$  [10], in which low spin  $d^5$   $\text{Ir}^{4+}$  ions reside on the vertices of a hyperkagome lattice, several theoretical studies for the classical ( $S \rightarrow \infty$ ) and quantum ( $S = 1/2$ ) Heisenberg antiferromagnet on such a lattice have been performed [11–19]. The main focus of these studies is at ground-state properties of the  $S = 1/2$  hyperkagome-lattice Heisenberg antiferromagnet. For the ground state of this model a gapped quantum spin liquid with topological order [12] and a gapless quantum spin liquid with spinon Fermi surfaces [15] were proposed by Lawler *et al.*. In contrast, Bergholtz *et al.* [16] proposed a valence bond crystal with a 72 site unit cell as the ground state of this model; this implies a spin gap with a huge number of singlet excitations below the lowest triplet state and thus a power law for the specific heat and a vanishing susceptibility for vanishing temperature.

Less attention has been paid to the finite-temperature properties of the  $S = 1/2$  hyperkagome-lattice Heisen-

berg antiferromagnet [15–17, 19]. It was argued that  $c(T) \propto T^2$  at low  $T$  [15] (similar to what is observed for  $\text{Na}_4\text{Ir}_3\text{O}_8$  [10]) and that  $\chi(T)$  has a non-zero value at  $T = 0$  and almost no temperature dependence as  $T \rightarrow 0$  [19] (again in agreement with experimental data for  $\text{Na}_4\text{Ir}_3\text{O}_8$  [10]). In addition, high-temperature series expansions for  $c$  and  $\chi$  were developed and compared with the experimental data for  $\text{Na}_4\text{Ir}_3\text{O}_8$  [17].

On the experimental side, apart from the mentioned iridate compound  $\text{Na}_4\text{Ir}_3\text{O}_8$  [10], there are other solid-state realizations of the hyperkagome-lattice Heisenberg antiferromagnet, see, e.g., Refs. [20–22]. Note, however, that the  $5d$ -based transition-metal oxides, such as  $\text{Na}_4\text{Ir}_3\text{O}_8$ , are known for having a large spin-orbit coupling so that the Heisenberg Hamiltonian apparently should be accomplished by other terms relevant for such materials [23].

In the present paper, we consider the thermodynamics of the  $S = 1/2$  hyperkagome-lattice Heisenberg antiferromagnet. The toolbox to tackle thermodynamics of frustrated quantum spin systems is rather scarce. Quantum Monte Carlo suffers from the sign problem [24], exact diagonalization or finite-temperature Lanczos methods are restricted to too small lattices [25–27], the density-matrix renormalization group technique requires a mapping via a “snake” path to a one-dimensional system [28]. Moreover, the pseudofermion functional renormalization group approach focuses on the wave-vector-dependent susceptibility [19], whereas one more universal method, the rotation-invariant Green’s function method [29–34], has not been applied to the  $S = 1/2$  hyperkagome-lattice Heisenberg antiferromagnet so far.

In our study, we use the high-temperature series expan-



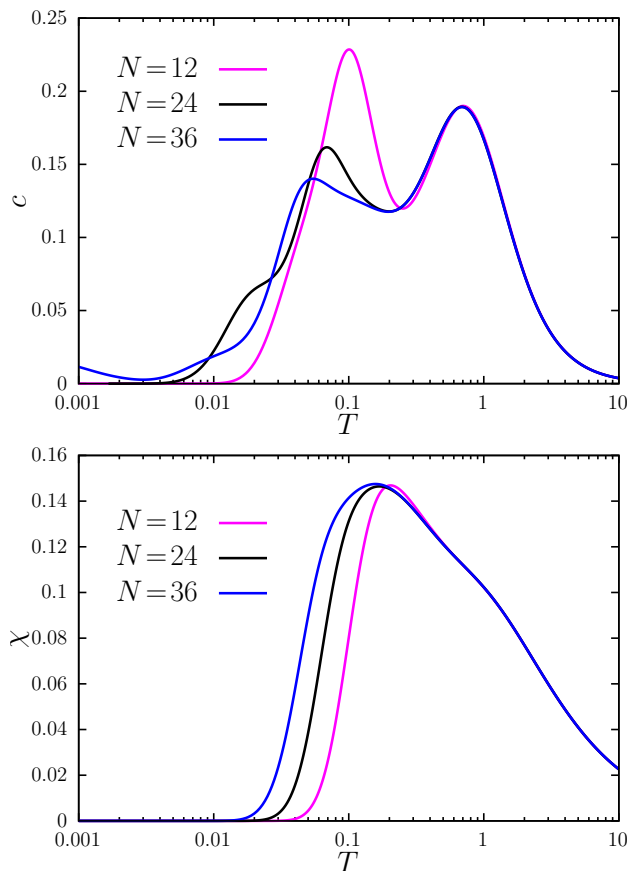


Figure 2. Finite-lattice results for (top) the specific heat and (bottom) the uniform susceptibility. Exact-diagonalization ( $N = 12$ ) and finite-temperature Lanczos method ( $N = 24$ ,  $R = 200$  and  $N = 36$ ,  $R = 20$ ) data. Details of calculations are given in Appendix A.

### III. NUMERICS FOR FINITE-SIZE LATTICES

Previously, exact-diagonalization and finite-temperature Lanczos methods were used for the  $S = 1/2$  pyrochlore-lattice Heisenberg antiferromagnet [41, 48]. At first glance, the hyperkagome-lattice case is simpler, since  $1/4$  of the pyrochlore sites are empty, however, the unit cell now contains 12 sites (instead of 4 sites for the pyrochlore) and the finite-system sizes may be  $N = 12, 24, 36, 48$ , and so on. The exact diagonalization for one unit cell with  $N = 12$  was reported in Ref. [15]. A chain-like arrangement of two ( $N = 24$ ) and three ( $N = 36$ ) unit cells is shown in Appendix A. Periodic boundary conditions are applied in all cases, also for  $N = 12$  in order to guarantee the correct number of nearest neighbors.

We report exact-diagonalization ( $N = 12$ ) and finite-temperature Lanczos ( $N = 24, 36$ ) data in Fig. 2. The results for the specific heat (top) and the uniform susceptibility (bottom) for  $N = 24$  and  $N = 36$  differ from each other below about  $T \approx 0.2$ . Surprisingly, the high-temperature peak of the specific heat does not show any

finite-size scaling; it is already provided by the calculations for one unit cell ( $N = 12$ ). On these grounds, we thus speculate that the curve of the specific heat at temperatures of the high-temperature peak and above represents the thermodynamic limit. The position of the low-temperature peak, on the other hand, does depend on the size; it is at  $T \approx 0.101$  for  $N = 12$ , at  $T \approx 0.069$  for  $N = 24$ , and at  $T \approx 0.055$  for  $N = 36$ . Moreover, the height decreases notably with growing  $N$ .

The maximum of  $\chi(T)$  has a mild dependence on system size; it occurs at  $T \approx 0.204$  for  $N = 12$ , at  $T \approx 0.168$  for  $N = 24$ , and at  $T \approx 0.158$  for  $N = 36$ . Moreover, the height remains practically unchanged. This behavior can be traced back to the size of the singlet-triplet gap for these systems. Its value is  $\Delta_{s-t} \approx 0.383, 0.216, 0.136$  for  $N = 12, 24, 36$ , respectively. The whole behavior is reminiscent of that of the kagome-lattice antiferromagnet [49].

In contrast, the results for the  $S = 1/2$  pyrochlore-lattice Heisenberg antiferromagnet of  $N = 32$  sites [41] reflect the thermodynamic limit only for  $T > 0.7$ , well above the temperature of the high-temperature peak of  $c(T)$ . Therefore, the finite-lattice results for the hyperkagome case allow a reliable discussion of thermodynamic properties for much lower temperatures down to  $T \approx 0.2$ . We provide more details in Sec. V on results.

### IV. ENTROPY METHOD

As have been mentioned above, in our study we use the high-temperature series expansion up to 16th order, which was reported in Ref. [17], see series expansion coefficients for  $\ln Z$  and the uniform structure factor in Table I of Ref. [17]. On the other hand, we employ the Magdeburg HTE code developed mainly by Lohmann [50, 51] (which is freely available at <http://www.uni-magdeburg.de/jschulen/HTE/>) in an extended version up to 13th order to check the series of the specific heat and the static uniform susceptibility. Our results coincide with those of Ref. [17].

The high-temperature series expansion may be improved by simple Padé approximants  $[u, d](T) = P_u(\beta)/Q_d(\beta)$ , where  $P_u(\beta)$  and  $Q_d(\beta)$  are polynomials of order  $u$  and  $d$ ,  $u + d \leq 16$ , and the series expansion of  $[u, d](T)$  coincides with the high-temperature series of  $c$  or  $\chi$  up to 16th order with respect to  $\beta = 1/T$ . Comparing close to diagonal Padé approximants [5, 5], [5, 6], [6, 6], [6, 7], [7, 7], [7, 8], [8, 8] (not shown here), we conclude that they start to deviate notably one from another below  $T \approx 0.5$  and thus can reproduce the high-temperature peak of  $c(T)$  at  $T \approx 0.669$ , but not any of the specific features of  $\chi(T)$  since  $\chi(T)$  increases monotonously to temperatures well below  $T = 0.5$  and also has got its maximum below  $T = 0.5$ .

In order to study the thermodynamic behavior at lower temperatures we use the entropy-method interpo-

lation scheme introduced by Bernu *et al.* [36–38] and further used in several studies [39–44]. Within the entropy method one interpolates the entropy (per site)  $s$  as a function of the mean (internal) energy (per site)  $e$ ,  $s(e)$ . As  $e$  approaches its maximal value  $e_\infty = E(T \rightarrow \infty)/N = \text{tr}(H)/N = 0$ , the entropy is known from high-temperature series expansion,  $s(e) = \ln 2 + \sum_{i>1} a_i e^i$  (i.e., the coefficients  $a_2, \dots, a_{16}$  are known, see Ref. [36]). As  $e$  approaches its minimal (ground-state) value  $e_0$ , the entropy behaves as  $s(e) \propto (e - e_0)^{\alpha/(1+\alpha)}$  if  $c(T) = AT^\alpha$  for  $T \rightarrow 0$  (gapless low-energy excitations) or as  $s(e) \propto -[(e - e_0)/\Delta](\ln[\Delta(e - e_0)] - 1)$  if  $c(T) \propto e^{-\Delta/T}/T^2$  for  $T \rightarrow 0$  (gapped low-energy excitations). Next, we interpolate, instead of  $s(e)$ , an auxiliary function  $G(e)$ , different for the two types of low-energy excitations, which immediately gives  $s(e)$ . For the gapless case we have

$$G(e) = \frac{[s(e)]^{\frac{1+\alpha}{\alpha}}}{e - e_0} \rightarrow G_{\text{app}}(e) = \frac{(\ln 2)^{\frac{\alpha}{1+\alpha}} P_u(e)}{-e_0 Q_d(e)}; \quad (2)$$

$$s_{\text{app}}(e) = [(e - e_0) G_{\text{app}}(e)]^{\frac{\alpha}{1+\alpha}}.$$

And for the gapped case we have

$$G(e) = (e - e_0) \left[ \frac{s(e)}{e - e_0} \right]' \rightarrow G_{\text{app}}(e) = \frac{\ln 2 P_u(e)}{e_0 Q_d(e)}; \quad (3)$$

$$\frac{s_{\text{app}}(e)}{e - e_0} = \frac{\ln 2}{-e_0} - \int_e^0 d\xi \frac{G_{\text{app}}(\xi)}{\xi - e_0}.$$

Here,  $P_u(e)$  and  $Q_d(e)$  are the polynomials of order  $u$  and  $d$ ,  $u + d \leq 16$ , and the series expansion of the quotient  $[u, d](e) = P_u(e)/Q_d(e)$  coincides with the Maclaurin series of  $G(e)$  known up to 16th order. Moreover, the prime denotes the derivative with respect to  $e$ . Knowing the dependence  $s(e)$ , we obtain the desired temperature dependence of the specific heat  $c(T)$  in the parametric form:  $T = 1/s'(e)$  and  $c = -[s'(e)]^2/s''(e)$ . Finally, we can calculate the prefactor  $A$ ,  $A_{\text{app}} = [\alpha^{1+\alpha}/(1+\alpha)^\alpha][G_{\text{app}}(e_0)]^\alpha$ , for the gapless case and the energy gap  $\Delta$ ,  $\Delta_{\text{app}} = -1/G_{\text{app}}(e_0)$ , for the gapped case. In the presence of a (small) external magnetic field  $h$  one gets the entropy  $s_{\text{app}}(e, h)$  which yields the uniform susceptibility  $\chi$  via the relations:  $m = [1/s'(e, h)]\partial s(e, h)/\partial h$ ,  $\chi = m/h$  ( $h \rightarrow 0$ ).

Thus, to obtain the thermodynamic quantities within the framework of the entropy method one needs, besides the high-temperature series for  $c$  and  $\chi$ , to know i) the ground-state energy  $e_0$ , ii) how  $c(T)$  vanishes as  $T \rightarrow 0$ , and iii) the value of  $\chi_0 \equiv \chi(T = 0)$  in the case of gapless low-energy excitations. Even if the precise value of  $e_0$  is not available and both gapless and gapped excitations are acceptable, one can proceed as in Ref. [40]. First, one has to assume some reasonable value  $e_0$  (being prepared to explore systematically a certain region of  $e_0$ ). Second, one has to assume the exponent  $\alpha$  in the case of a gapless spectrum or one has to assume that the spectrum is gapped. Then, for the assumed  $e_0$  and gapless/gapped energy spectrum one has to calculate within the entropy method the specific heat  $c(T)$  using all  $n_P$

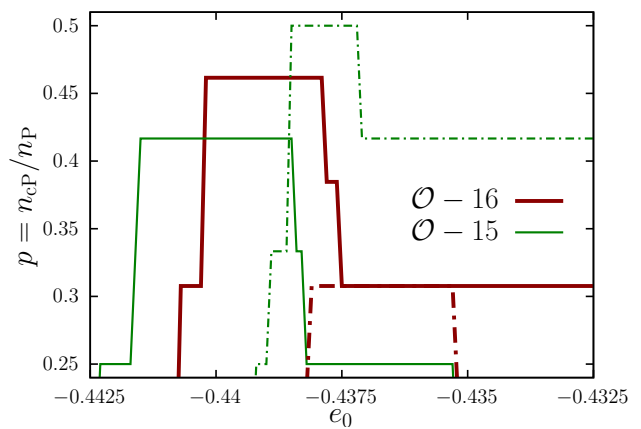


Figure 3. The ratio of the number of “coinciding” entropy-method Padé approximants  $n_{cP}$  to the number of all considered entropy-method Padé approximants  $n_P$ ,  $p = n_{cP}/n_P$ , based on the series of 15th (thin green) and 16th (thick red) orders as a function of the chosen value of  $e_0$ . Here  $T_i = 0.5$ ,  $\Delta T = 0.025$ ,  $T_f = 0.1$ , see the main text. We consider both assumptions, gapless (solid) and gapped (dot-dashed) low-energy excitations.

available Padé approximants  $[u, d](e)$ . There are  $n + 1$  Padé approximants based on the series up to  $n$ th order; we discard from the very beginning four Padé approximants  $[n, 0]$ ,  $[n - 1, 1]$ ,  $[1, n - 1]$ ,  $[0, n]$  so that  $n_P = n - 3$ . Next, one has to examine the “closeness” of all  $n_P$  profiles  $c(T)$  by examining them thoroughly from some (high enough, but not too high) temperature  $T_i$  down to some (sufficiently low) temperature  $T_f$  with temperature steps  $\Delta T$ . If the absolute value of the difference of a certain  $c$  from the average value (arithmetic mean)  $\bar{c}$  at a running temperature  $T$  ( $T_f \leq T \leq T_i$ ) is less than some bound, e.g., 0.001, this  $c$  belongs to the set of “coinciding” Padé approximants. In the opposite case, this Padé approximant is discarded and not considered for lower temperatures. According to Refs. [40, 43], a large number of coinciding curves  $n_{cP}$ , or more precisely a large value of  $p = n_{cP}/n_P$ , provides evidence that the assumptions made about  $e_0$  and the low-energy excitations are self-consistent.

In Fig. 3 we illustrate such an analysis based on  $n_P$  Padé approximants following from the 15th (thin green) and 16th order (thick red) in Eqs. (2) or (3) for the specific heat  $c(T)$  under the assumption of a gapless spectrum with  $\alpha = 2$  (solid) or a gapped spectrum (dot-dashed). Here we set  $T_i = 0.5$ ,  $\Delta T = 0.025$ ,  $T_f = 0.1$ , see Appendix B. If  $e_0$  is taken in the range  $-0.4402 \dots -0.4379$  assuming a gapless spectrum, i.e.,  $c(T) = AT^2$  as  $T \rightarrow 0$ , and the analysis is based on 16th order ( $n_P = 13$ ), we find that  $n_{cP} = 6$  and  $p \approx 0.46$ . Moreover, for the prefactor  $A$  we get  $A = 493 \dots 727$ . If  $e_0$  is taken in the range  $-0.4381 \dots -0.4353$  assuming a gapped spectrum and the analysis is based on 16th order, we find  $p = 4/13 \approx 0.31$ . Moreover, the energy gap is  $\Delta = 0.025 \dots 0.018$ . All these find-

Table I. Ground-state energy  $e_0$  obtained by different authors

$N=12$ [15]	-0.454
$N=12/24/36$ (present paper)	-0.453 74/-0.446 33/-0.445 10
QSL [15]	-0.424
VBC [16]	-0.430 115
EM (present paper)	-0.440 ... -0.435

ings are visualized by the thick red curves in Fig. 3. Slightly different values of  $e_0$  which provide maximal values of  $p$  follow from the analysis based on 15th order, see the thin green curves in Fig. 3. Namely, for the gapless spectrum with  $e_0 = -0.4415\dots -0.4385$  we have  $p = 5/12 \approx 0.42$ ,  $A = 377\dots 563$ ; for the gapped spectrum with  $e_0 = -0.4385\dots -0.4372$  we have  $p = 6/12 = 0.5$ ,  $\Delta = 0.027\dots 0.024$ .

Following the strategy of Refs. [40, 43], we may conclude that the entropy-method prediction for the ground-state energy  $e_0$  is  $-0.4402\dots -0.4379$  (gapless excitations) or  $-0.4381\dots -0.4353$  (gapped excitations). By combination of both cases we arrive at  $e_0 = -0.440\dots -0.435$ . In what follows we use this missing input parameter  $e_0$  for the entropy method, considering both assumptions about  $c(T)$  as  $T \rightarrow 0$ . We note in passing that the uniform susceptibility  $\chi(T)$  is less convenient for seeking a large value of  $p = n_{cP}/n_P$ , since it requires the additional parameter  $\chi_0$  if the spectrum is gapless.

## V. RESULTS

### A. Ground-state energy $e_0$

We begin with the discussion of the ground-state energy of the  $S = 1/2$  hyperkagome-lattice Heisenberg antiferromagnet. Various proposals about the nature of the ground state, i.e., spin liquids or valence-bond crystals, yield for  $e_0$  the values  $-0.430\dots -0.424$ , see Table I. Exact diagonalizations for  $N = 12, 24, 36$  yield  $-0.45374$ ,  $-0.44633$ ,  $-0.44510$ , see Table I, that, apparently, are overestimated values of the thermodynamically large systems. As explained above, to provide consistency of the entropy-method calculations, we have to assume for  $e_0$  the values  $-0.440\dots -0.435$ . Yet another plausible simple approach to determine  $e_0$  from the high-temperature series expansion [6] is discussed in Appendix C; it yields  $e_0$  about  $-0.448$ . The determination of  $e_0$  based on the high-temperature series expansion seems to be rather formal, since it does not use any specific picture for the ground state. However, the experience from other models, including exactly solvable ones and precisely examined numerically ones, gives hints that it may yield quite reasonable predictions [40, 43].

It is worth noting that the ground-state energy for the kagome lattice is quite close:  $-0.4386(5)$  [52, 53],  $-0.4387\dots$  [54] (i.e., about  $-0.219$  per bond), but for

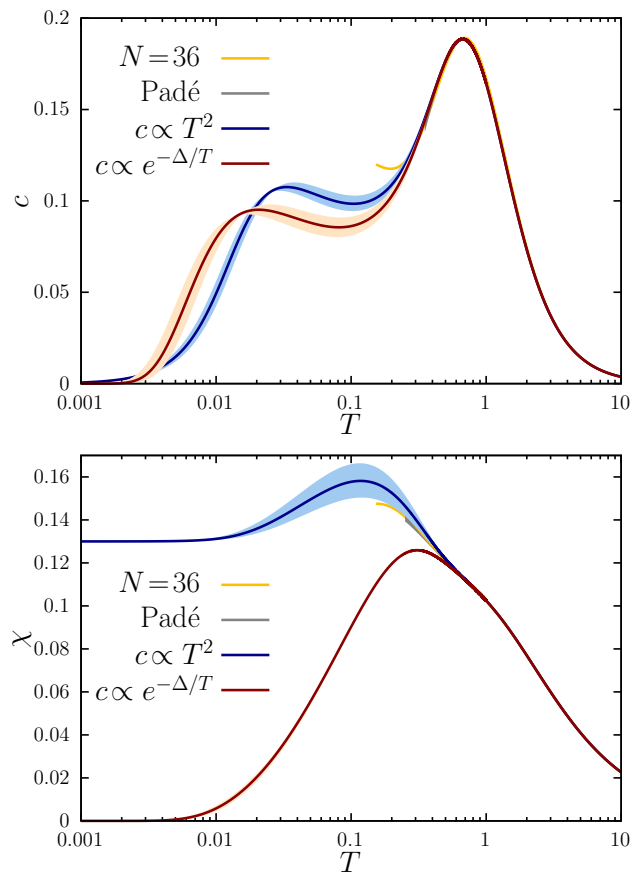


Figure 4. Entropy-method results, obtained as explained in Sec. IV, for (top) the specific heat and (bottom) the uniform susceptibility of the hyperkagome-lattice  $S = 1/2$  Heisenberg antiferromagnet. Blue curves correspond to the gapless spectrum  $c = AT^2$  and red ones to the gapped spectrum  $c \propto e^{-\Delta/T}/T^2$ . The shaded area (light blue and light red) represents the region of  $e_0$  where  $p$  has a maximum (see Fig. 3). We also show  $N = 36$  data (yellow) and two simple Padé approximants [7, 7] and [8, 8] for  $c(T)$  ( $T \geq 0.35$ ) and for  $\chi(T)$  ( $T \geq 0.25$ ) and color in gray the region between them. The simple Padé approximants almost coincide with the entropy-method curves especially in the top panel. In the case of gapless excitations, we set  $\chi_0 = 0.13$ .

the pyrochlore lattice it is rather different:  $-0.490(6)$  [6],  $-0.4831(1)$  [7],  $-0.489\dots$  [9] (i.e., about  $-0.163$  per bond).

### B. Thermodynamic properties

We pass to finite-temperature properties of the  $S = 1/2$  hyperkagome-lattice Heisenberg antiferromagnet. In Fig. 4 we report the temperature dependence of the specific heat and the uniform susceptibility obtained by the entropy-method. The ground-state energy is determined from the analysis of  $c(T)$  as was explained in Sec. IV. Both possibilities, the gapless spectrum with  $\alpha = 2$  and the gapped spectrum, were considered, see blue and red

curves, respectively. For the gapless excitations we set  $\chi_0 = 0.13$  inspired by experimental data [10] and other theoretical papers [17, 19].

The specific heat  $c(T)$  besides the high-temperature peak at  $T \approx 0.669$  has an additional low-temperature one at about  $T \approx 0.033$  (gapless excitations) or  $T \approx 0.021$  (gapped excitations); the height of the low-temperature peak is about two times smaller than the height of the main peak. These features, at least at intermediate temperatures and above, are quite similar to what is known for the kagome-lattice (and also the square-kagome-lattice) case (a peak at  $T = 0.67$ , a shoulder of two times smaller height at  $T = 0.1 \dots 0.25$  [49, 55]), but differ from those for the pyrochlore-lattice case, where only one maximum in  $c(T)$ , but no additional low-temperature feature (peak/shoulder) was found [41, 56]. Concerning high-temperature series expansions for  $c$ , they coincide for the hyperkagome and kagome lattices up to  $\beta^5$ , but differ for the pyrochlore lattice already in terms proportional to  $\beta^2$ .

The uniform susceptibility  $\chi(T)$  behaves identically at  $T$  above about 0.5 for gapless and gapped excitations. For lower temperatures,  $\chi(T)$  has a maximum at  $T \approx 0.118$  (gapless excitations) or  $T \approx 0.309$  (gapped excitations) and approaches either  $\chi_0$  (the former case) or zero (the latter case) as the temperature goes to zero. This resembles the maximum of  $\chi(T)$  for the finite-size kagome lattices [49] and for the infinite kagome lattice analysed by the entropy method [38]. In contrast, for the pyrochlore lattice we have several scenarios none of which can be excluded to date [41, 56, 57]. Concerning high-temperature series expansions for  $\chi$ , they coincide for the hyperkagome- and kagome-lattice cases up to  $\beta^6$  but differ for the pyrochlore-lattice case already in terms proportional to  $\beta^3$ .

A general message that can be taken from Fig. 4 is that the entropy-method and finite-system numerics data (and even simple Padé approximants for  $\chi$ ) favour the assumption of a gapless spectrum. This conclusion agrees with experiments for  $\text{Na}_4\text{Ir}_3\text{O}_8$ .

As has been mentioned above, the hyperkagome-lattice Heisenberg antiferromagnet has similar properties with the kagome-lattice one, but different to the pyrochlore-lattice one. In Fig. 5 we compare the finite-temperature Lanczos method data for  $c(T)$  and  $\chi(T)$  for the hyperkagome-lattice case with the kagome- and pyrochlore-lattice cases. We have to remark here that the energy scale is different for the pyrochlore (each site has six neighbors) and the kagome or hyperkagome (each site has four neighbors) and one may rescale  $T \rightarrow T/z$  and  $\chi \rightarrow \chi z$  so that different lattices, with  $z = 4$  and  $z = 6$ , can be compared, but the conclusions below remain unchanged. Namely, Fig. 5 illustrates a good agreement above about  $T = 0.25$  for the specific heat (top panel) and even for all temperatures for the uniform susceptibility (bottom panel) for the hyperkagome- and kagome-lattice Heisenberg antiferromagnets. In contrast, the pyrochlore-lattice Heisenberg antiferromagnet

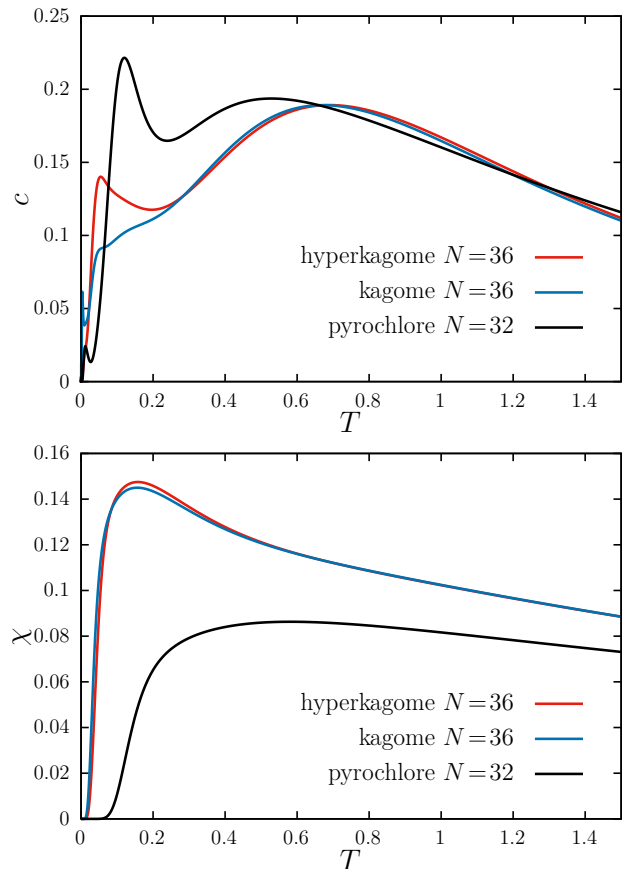


Figure 5. Comparison with the kagome- and pyrochlore-lattice cases for (top) the specific heat and (bottom) the uniform susceptibility. Finite-temperature Lanczos method data for  $N = 36$  (hyperkagome lattice, see Fig. 2, and kagome lattice [49]) and  $N = 32$  (pyrochlore lattice [41]). The extra low-temperature peak of  $c(T)$  at  $T \approx 0.117$  for the pyrochlore lattice (top panel, black curve) is a finite-size effect and is not present for  $N \rightarrow \infty$  [41].

shows different temperature profiles  $c(T)$  and  $\chi(T)$  (also after rescaling). Thus, we may conclude that the three-dimensional hyperkagome lattice is closer to highly frustrated two-dimensional lattices (kagome, square-kagome) than to the three-dimensional pyrochlore lattice. However, it is worth noting the difference: For the kagome lattice the low-temperature peak of  $c(T)$  moves to higher temperatures with increasing  $N$  [49], opposite to what is observed for the hyperkagome lattice (recall the top panel of Fig. 2). Thus, for the kagome lattice one yields a low-temperature shoulder of the main peak in the thermodynamic limit [58].

Before closing this section, let us comment on the relevance for experiments. Previous theoretical papers [15, 17, 19] compare  $c(T)$  or  $c(T)/T$  and  $\chi(T)$  or  $1/\chi(T)$  to available experimental data for the  $S = 1/2$  hyperkagome antiferromagnet  $\text{Na}_4\text{Ir}_3\text{O}_8$  [10]. These comparisons exhibit noticeable discrepancies roughly below  $J/2$  ( $J$  is about 300 K for  $\text{Na}_4\text{Ir}_3\text{O}_8$ ) and even at higher tem-

peratures for the specific heat. The authors attributed this disagreement to an incomplete subtraction of non-magnetic contribution to the experimentally measured  $c(T)$  [17] and an insufficiency of the model (1) for description of the  $S = 1/2$  hyperkagome antiferromagnet  $\text{Na}_4\text{Ir}_3\text{O}_8$  [16, 23].

## VI. SUMMARY

In the present paper, we consider the  $S = 1/2$  hyperkagome-lattice Heisenberg antiferromagnet. Using finite-lattice calculations and high-temperature series expansion up to 16th order [17] complemented by plausible assumptions about low-temperature properties we have obtained the temperature dependences for the specific heat and the uniform susceptibility. Our main findings are as follows: We observe a two-peak profile for  $c(T)$ , and we do not see any difference on whether the excitations are gapless or gapped for  $\chi(T)$  above  $T \approx 0.5$ . As a byproduct, we obtain the ground state energy  $e_0$ , which provides self-consistency of the entropy-method calculations. We have found that the thermodynamics of the three-dimensional hyperkagome-lattice Heisenberg antiferromagnet is quite similar to the two-dimensional kagome-lattice one, but differs from that of the pyrochlore lattice.

Future work on thermodynamics may be related to application of universal and specific tools to tackle the problem. Evidently, the  $S = 1/2$  hyperkagome-lattice Heisenberg antiferromagnet can be studied by the rotation-invariant Green's function method for obtaining approximate thermodynamic and dynamic quantities on an equal footing. Similar studies for the quantum kagome-lattice and pyrochlore-lattice Heisenberg antiferromagnets were reported in Refs. [33, 34]. On the other hand, the hyperkagome-lattice Heisenberg antiferromagnet represents a flat-band system, since the one-magnon energy spectrum has dispersionless (flat) bands. The flat-band states may be relevant at high fields and low temperatures and their dominant contribution to thermodynamics can be elaborated by special methods of flat-band systems, see Refs. [59, 60].

## ACKNOWLEDGEMENTS

T. H. was supported by the fellowship of the President of Ukraine for young scholars and by the Projects of research works of young scientists of the National Academy of Sciences of Ukraine (project # 29-04/18-2023, Frustrated quantum magnets at finite temperatures). O. D. thanks J. Strečka for the kind hospitality at the MECO48 conference (Stará Lesná, Slovakia, May 22-26, 2023). O. D. acknowledges the kind hospitality of the University of Bielefeld in October-December of 2023 (supported by Erasmus+ and DFG). This work was supported by the

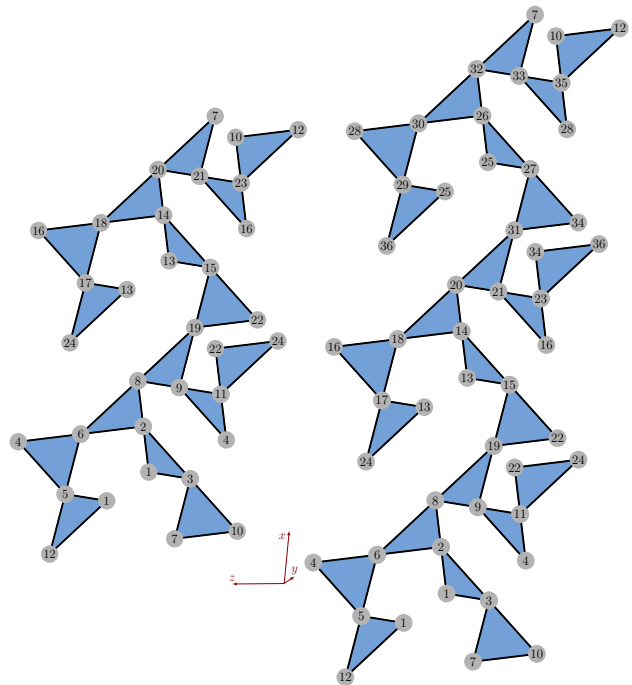


Figure 6. Finite-size hyperkagome lattices with (left)  $N = 24$  and (right)  $N = 36$  for finite-temperature Lanczos method studies.

Deutsche Forschungsgemeinschaft (DFG SCHN 615/28-1 and RI 615/25-1).

## Appendix A: Finite-lattice calculations

In this appendix we present more details about finite-lattice calculations. For exact diagonalizations, we use the 12-site unit cell with periodic boundary conditions. Note that the open 12-site unit cell has sites with only two neighbors, as, e.g., site 1, since the bonds between this site and sites 2 and 3 are absent for open boundary conditions. Periodic boundary conditions appear after superposing the sites 1 and  $1 + y$ , 4 and  $4 + z$ , 8 and  $8 - x$ , 9 and  $9 - x$ , 10 and  $10 + z$ , 11 and  $11 - x + y + z$ , 12 and  $12 + y$  in Fig. 1. In Fig. 6 we show the lattices of 24 and 36 sites (two and three unit cells arranged in a row along the  $x$  axis) which are used for studies with the finite-temperature Lanczos method. In Fig. 6, the sites  $1, \dots, 12$  of the first unit cell (cf. Fig. 1) are numbered as  $13, \dots, 24$  and  $25, \dots, 36$  in the second and third unit cell, respectively. Periodic boundary conditions are implied in  $x$ ,  $y$ , and  $z$  directions, i.e., the gray disks with identical numbers in Fig. 6 coincide.

In our finite-lattice numerics we use the conservation of the  $z$ -component of the total spin as well as lattice symmetries, i.e., the Hilbert space  $\mathcal{H}$  splits into orthogonal subspaces  $\mathcal{H}(\gamma)$  with  $\gamma$  labeling the respective symmetry. Exact and complete diagonalizations are performed for  $N = 12$  using Schulenburg's publicly available package

*spinpack* [61, 62].

Within the finite-temperature Lanczos method, the sum over an orthonormal basis in the partition function  $Z$  is replaced in a Monte-Carlo fashion by a much smaller sum over  $R$  random vectors where each random vector is employed for a trace estimation [25],

$$Z \approx \sum_{\gamma=1}^{\Gamma} \frac{\dim(\mathcal{H}(\gamma))}{R} \sum_{\nu=1}^R \sum_{n=1}^{N_L} \exp\left(-\frac{\epsilon_n^{(\nu)}}{T}\right) \times | \langle n(\nu) | \nu \rangle |^2, \quad (\text{A1})$$

where  $|\nu\rangle$  labels random vectors for each symmetry-related orthogonal subspace  $\mathcal{H}(\gamma)$ . The exponential of the Hamiltonian  $H$  in Eq. (A1) is approximated by its spectral representation in a Krylov space spanned by the  $N_L$  Lanczos vectors starting from the respective random vector  $|\nu\rangle$ , where  $|n(\nu)\rangle$  is the  $n$ th eigenvector of  $H$  in this Krylov space with the energy  $\epsilon_n^{(\nu)}$ . In the present study we take  $R = 200$  for  $N = 24$  and  $R = 20$  for  $N = 36$ , cf. Fig. 2.

### Appendix B: More details of the entropy-method calculations

In this appendix we provide some technical details about the entropy-method calculations which are outlined in Sec. IV. Our approach is similar to the one of Refs. [40, 43].

First we construct for a reference a bundle of close to diagonal Padé approximants  $[u, d](T)$  of the high-temperature series for  $c(T)$  and select those Padé approximants which are “indistinguishable” unless the temperature becomes lower than, say,  $T = 0.5$ . Clearly, the entropy-method profiles  $c(T)$  should coincide with the bundle of simple Padé approximants above this temperature. Next, we take the initial temperature  $T_i = 0.5$  at which the constructed simple Padé approximants begin to deviate one from another and start to lower the temperature by  $\Delta T = 0.025$  making 16 steps to reach the final temperature  $T_f = 0.1$ . We assume a certain value of  $e_0$  (and will scan the ground-state energies  $e_0$  with the step  $\Delta e_0 = 0.0001$ ), and consider both scenarios for the low-energy spectrum (gapped or gapless) separately. This way, we obtain a set of entropy-method curves  $c(T)$  according to all considered  $n_P$  Padé approximants  $[u, d](e)$  in Eqs. (2) or (3). The entropy-method curves  $c(T)$  coincide with the bundle of simple Padé approximants for  $T \geq T_i$  with the absolute accuracy below, e.g., 0.001. Now, for each temperature  $T_i, T_i - \Delta T, \dots, T_f$ , we find those  $[u, d](e)$  that yield  $c(T)$  which deviates from the average value (arithmetic mean)  $\overline{c(T)}$  by an absolute value less than 0.001. We count the number of such Padé approximants  $n_{cP}$  and calculate  $p = n_{cP}/n_P$ .

In Sec. IV we mention that the choice of  $T_i$  is important: We took  $T_i = 0.5$  which is below the temperature of the high-temperature peak of  $c(T)$  at  $T \approx 0.669$ . We

also like to remark that achieving large values of the ratio  $p = n_{cP}/n_P$  should be considered with caution. For example, if taking  $T_i = 1$  (and  $\Delta T = 0.05$ ,  $T_f = 0.2$ ), we obtain values of  $p$  quite close to 1 (above 0.69 and up to 0.92). However, by comparing the related curves of  $c(T)$  and  $\chi(T)$  with simple Padé approximants one notices a larger discrepancies at  $T = 0.5$  than in Fig. 4. Therefore, since simple Padé approximants converge well above  $T \approx 0.5$  we conclude that the choice of  $T_i = 0.5$  is preferable.

### Appendix C: Estimation of $e_0$ from high-temperature series expansion

The high-temperature series expansion can be used for the estimation of the ground-state energy of the  $S = 1/2$  hyperkagome-lattice Heisenberg antiferromagnet following the lines of the Supplementary Material of Ref. [6]. Below we repeat these arguments for the  $S = 1/2$  hyperkagome-lattice Heisenberg antiferromagnet.

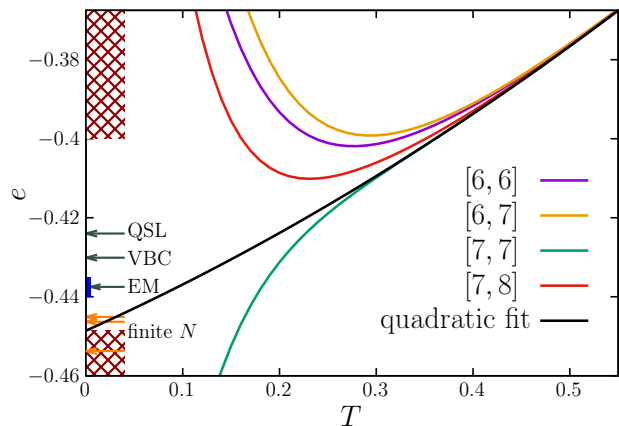


Figure 7. Estimate of the ground-state energy  $e_0$  from the high-temperature series expansion up to 16th order (black curve). We also plot simple Padé approximants for the internal energy  $e = (-\partial \ln Z / \partial \beta) / N$  and show the results for  $e_0$  of Refs. [15, 16] along with the entropy-method and finite  $N$  data for  $e_0$ , see Table I.

Since  $c(T) = \partial e(T) / \partial T$ , the ground-state energy  $e_0$  is given by  $e_0 = -\int_0^\infty dT c(T)$ . Moreover, its upper bound is given by  $e_0^* = -\int_{T^*}^\infty dT c(T)$ , where  $T^* > 0$  is a temperature above which simple Padé approximants  $[u, d](T)$  of the high-temperature series expansion of  $c(T)$  show a reliable convergence. Replacing  $c(T)$  by  $[8, 8](T)$  and assuming  $T^* = 0.35$  we obtain for the upper bound  $e_0^* \approx -0.401$ , see Fig. 7.

Furthermore, consider the  $e(T)$  as it is given by the  $[7, 8](T)$  Padé approximant and fit  $e(T)$  by a quadratic polynomial  $e_0 + e_1 T + e_2 T^2$  in the range between  $T = 0.4$  and  $T = 0.5$  or between  $T = 0.4$  and  $T = 0.55$ . This way we get an estimate for the ground-state energy

$e_0 \approx -0.448$ , see Fig. 7. If the taken range is between  $T = 0.35$  and  $T = 0.55$ , we arrive at only about 0.1%

lower energy  $e_0$ . Just this latter quadratic fit is shown by the black curve in Fig. 7. In Fig. 7 we also compare different predictions for  $e_0$ .

- 
- [1] C. Berthier, L. P. Lévy, and G. Martinez, eds., *High Magnetic Fields: Applications in Condensed Matter Physics and Spectroscopy*, Vol. 595 (Springer Berlin, Heidelberg, 2002).
- [2] U. Schöllwöck, J. Richter, D. J. J. Farnell, and R. F. Bishop, eds., *Quantum Magnetism*, Vol. 645 (Springer Berlin, Heidelberg, 2004).
- [3] H. T. Diep, ed., *Frustrated Spin Systems* (World Scientific, Singapore, 2005).
- [4] C. Lacroix, P. Mendels, and F. Mila, *Introduction to Frustrated Magnetism – Materials, Experiments, Theory*, Springer Series in Solid-State Sciences, Vol. 164 (Springer, Berlin, Heidelberg, 2011).
- [5] B. Canals and C. Lacroix, Pyrochlore Antiferromagnet: A Three-Dimensional Quantum Spin Liquid, *Phys. Rev. Lett.* **80**, 2933 (1998).
- [6] I. Hagymási, R. Schäfer, R. Moessner, and D. J. Luitz, Possible Inversion Symmetry Breaking in the  $S = 1/2$  Pyrochlore Heisenberg Magnet, *Phys. Rev. Lett.* **126**, 117204 (2021).
- [7] N. Astrakhantsev, T. Westerhout, A. Tiwari, K. Choo, A. Chen, M. H. Fischer, G. Carleo, and T. Neupert, Broken-Symmetry Ground States of the Heisenberg Model on the Pyrochlore Lattice, *Phys. Rev. X* **11**, 041021 (2021).
- [8] M. Hering, V. Nocolak, F. Ferrari, Y. Iqbal, and J. Reuther, Dimerization tendencies of the pyrochlore Heisenberg antiferromagnet: A functional renormalization group perspective, *Phys. Rev. B* **105**, 054426 (2022).
- [9] R. Schäfer, B. Placke, O. Benton, and R. Moessner, Abundance of Hard-Hexagon Crystals in the Quantum Pyrochlore Antiferromagnet, *Phys. Rev. Lett.* **131**, 096702 (2023).
- [10] Y. Okamoto, M. Nohara, H. Aruga-Katori, and H. Takagi, Spin-Liquid State in the  $S = 1/2$  Hyperkagome Antiferromagnet  $\text{Na}_4\text{Ir}_3\text{O}_8$ , *Phys. Rev. Lett.* **99**, 137207 (2007).
- [11] J. M. Hopkinson, S. V. Isakov, H.-Y. Kee, and Y. B. Kim, Classical Antiferromagnet on a Hyperkagome Lattice, *Phys. Rev. Lett.* **99**, 037201 (2007).
- [12] M. J. Lawler, H.-Y. Kee, Y. B. Kim, and A. Vishwanath, Topological Spin Liquid on the Hyperkagome Lattice of  $\text{Na}_4\text{Ir}_3\text{O}_8$ , *Phys. Rev. Lett.* **100**, 227201 (2008).
- [13] M. E. Zhitomirsky, Octupolar ordering of classical kagome antiferromagnets in two and three dimensions, *Phys. Rev. B* **78**, 094423 (2008).
- [14] Y. Zhou, P. A. Lee, T.-K. Ng, and F.-C. Zhang,  $\text{Na}_4\text{Ir}_3\text{O}_8$  as a 3D Spin Liquid with Fermionic Spinons, *Phys. Rev. Lett.* **101**, 197201 (2008).
- [15] M. J. Lawler, A. Paramekanti, Y. B. Kim, and L. Balents, Gapless Spin Liquids on the Three-Dimensional Hyperkagome Lattice of  $\text{Na}_4\text{Ir}_3\text{O}_8$ , *Phys. Rev. Lett.* **101**, 197202 (2008).
- [16] E. J. Bergholtz, A. M. Läuchli, and R. Moessner, Symmetry Breaking on the Three-Dimensional Hyperkagome Lattice of  $\text{Na}_4\text{Ir}_3\text{O}_8$ , *Phys. Rev. Lett.* **105**, 237202 (2010).
- [17] R. R. P. Singh and J. Oitmaa, High-temperature series expansion study of the Heisenberg antiferromagnet on the hyperkagome lattice: Comparison with  $\text{Na}_4\text{Ir}_3\text{O}_8$ , *Phys. Rev. B* **85**, 104406 (2012).
- [18] Y. Wan and Y. B. Kim, Phenomenological approach to a hyperkagome spin liquid: Emergent gauge fields and spinons, *Phys. Rev. B* **94**, 224401 (2016).
- [19] F. L. Buessen and S. Trebst, Competing magnetic orders and spin liquids in two- and three-dimensional kagome systems: Pseudofermion functional renormalization group perspective, *Phys. Rev. B* **94**, 235138 (2016).
- [20] B. Koteswararao, R. Kumar, P. Khuntia, S. Bhowal, S. K. Panda, M. R. Rahman, A. V. Mahajan, I. Dasgupta, M. Baenitz, K. H. Kim, and F. C. Chou, Magnetic properties and heat capacity of the three-dimensional frustrated  $S = \frac{1}{2}$  antiferromagnet  $\text{PbCuTe}_2\text{O}_6$ , *Phys. Rev. B* **90**, 035141 (2014).
- [21] S. Chillal, Y. Iqbal, H. O. Jeschke, J. A. Rodriguez-Rivera, R. Bewley, P. Manuel, D. Khalyavin, P. Steffens, R. Thomale, A. T. M. N. Islam, J. Reuther, and B. Lake, Evidence for a three-dimensional quantum spin liquid in  $\text{PbCuTe}_2\text{O}_6$ , *Nature Communications* **11**, 2348 (2020).
- [22] B. Sana, M. Barik, M. Pregelj, U. Jena, M. Baenitz, J. Sichelschmidt, K. Sethupathi, and P. Khuntia, Magnetic properties of a spin-orbit entangled  $J_{\text{eff}} = \frac{1}{2}$  three-dimensional frustrated rare-earth hyperkagome material, *Phys. Rev. B* **108**, 134413 (2023).
- [23] B. Huang, Y. B. Kim, and Y.-M. Lu, Interplay of nonsymmorphic symmetry and spin-orbit coupling in hyperkagome spin liquids: Applications to  $\text{Na}_4\text{Ir}_3\text{O}_8$ , *Phys. Rev. B* **95**, 054404 (2017).
- [24] P. Henelius and A. W. Sandvik, Sign problem in Monte Carlo simulations of frustrated quantum spin systems, *Phys. Rev. B* **62**, 1102 (2000).
- [25] J. Jaklič and P. Prelovšek, Lanczos method for the calculation of finite-temperature quantities in correlated systems, *Phys. Rev. B* **49**, 5065 (1994).
- [26] R. Schnalle and J. Schnack, Calculating the energy spectra of magnetic molecules: application of real- and spin-space symmetries, *Int. Rev. Phys. Chem.* **29**, 403 (2010).
- [27] J. Schnack, J. Richter, and R. Steinigeweg, Accuracy of the finite-temperature Lanczos method compared to simple typicality-based estimates, *Phys. Rev. Research* **2**, 013186 (2020).
- [28] J. Ummethum, J. Schnack, and A. Läuchli, Large-scale numerical investigations of the antiferromagnetic Heisenberg icosidodecahedron, *J. Magn. Magn. Mater.* **327**, 103 (2013).
- [29] J. Kondo and K. Yamaji, Green's-function formalism of the one-dimensional Heisenberg spin system, *Prog. Theor. Phys.* **47**, 807 (1972).
- [30] H. Shimahara and S. Takada, Green's function theory of the two-dimensional Heisenberg model - spin wave in short range order -, *J. Phys. Soc. Jpn.* **60**, 2394 (1991).
- [31] A. F. Barabanov and V. M. Beresovsky, On the theory

- of the two-dimensional Heisenberg antiferromagnet with frustration on a square lattice, *J. Phys. Soc. Jpn.* **63**, 3974 (1994).
- [32] S. Winterfeldt and D. Ihle, Theory of antiferromagnetic short-range order in the two-dimensional Heisenberg model, *Phys. Rev. B* **56**, 5535 (1997).
- [33] P. Müller, A. Zander, and J. Richter, Thermodynamics of the kagome-lattice Heisenberg antiferromagnet with arbitrary spin  $S$ , *Phys. Rev. B* **98**, 024414 (2018).
- [34] P. Müller, A. Lohmann, J. Richter, and O. Derzhko, Thermodynamics of the pyrochlore-lattice quantum Heisenberg antiferromagnet, *Phys. Rev. B* **100**, 024424 (2019).
- [35] Temperatures are given as multiples of the exchange interaction.  $T = 0.25$  thus means  $k_B T/J = 0.25$ .
- [36] B. Bernu and G. Misguich, Specific heat and high-temperature series of lattice models: Interpolation scheme and examples on quantum spin systems in one and two dimensions, *Phys. Rev. B* **63**, 134409 (2001).
- [37] G. Misguich and B. Bernu, Specific heat of the  $S = \frac{1}{2}$  Heisenberg model on the kagome lattice: High-temperature series expansion analysis, *Phys. Rev. B* **71**, 014417 (2005).
- [38] B. Bernu and C. Lhuillier, Spin Susceptibility of Quantum Magnets from High to Low Temperatures, *Phys. Rev. Lett.* **114**, 057201 (2015).
- [39] H.-J. Schmidt, A. Hauser, A. Lohmann, and J. Richter, Interpolation between low and high temperatures of the specific heat for spin systems, *Phys. Rev. E* **95**, 042110 (2017).
- [40] B. Bernu, L. Pierre, K. Essafi, and L. Messio, Effect of perturbations on the kagome  $S = \frac{1}{2}$  antiferromagnet at all temperatures, *Phys. Rev. B* **101**, 140403 (2020).
- [41] O. Derzhko, T. Hutak, T. Krokhumalskii, J. Schnack, and J. Richter, Adapting Planck's route to investigate the thermodynamics of the spin-half pyrochlore Heisenberg antiferromagnet, *Phys. Rev. B* **101**, 174426 (2020).
- [42] V. Grison, P. Viot, B. Bernu, and L. Messio, Emergent Potts order in the kagome  $J_1 - J_3$  Heisenberg model, *Phys. Rev. B* **102**, 214424 (2020).
- [43] M. G. Gonzalez, B. Bernu, L. Pierre, and L. Messio, Ground-state and thermodynamic properties of the spin- $\frac{1}{2}$  Heisenberg model on the anisotropic triangular lattice, *SciPost Phys.* **12**, 112 (2022).
- [44] T. Hutak, T. Krokhumalskii, O. Derzhko, and J. Richter, Spin-half Heisenberg antiferromagnet on a symmetric sawtooth chain: rotation-invariant Green's functions and high-temperature series, *Eur. Phys. J. B* **96**, 50 (2023).
- [45] H.-K. Jin and Y. Zhou, Classical and quantum order in hyperkagome antiferromagnets, *Phys. Rev. B* **101**, 054408 (2020).
- [46] L. E. Chern and Y. B. Kim, Theoretical study of quantum spin liquids in  $s = \frac{1}{2}$  hyper-hyperkagome magnets: Classification, heat capacity, and dynamical spin structure factor, *Phys. Rev. B* **104**, 094413 (2021).
- [47] R. Pohle and L. D. C. Jaubert, Curie-law crossover in spin liquids, *Phys. Rev. B* **108**, 024411 (2023).
- [48] V. R. Chandra and J. Sahoo, Spin- $\frac{1}{2}$  Heisenberg antiferromagnet on the pyrochlore lattice: An exact diagonalization study, *Phys. Rev. B* **97**, 144407 (2018).
- [49] J. Schnack, J. Schulenburg, and J. Richter, Magnetism of the  $N = 42$  kagome lattice antiferromagnet, *Phys. Rev. B* **98**, 094423 (2018).
- [50] H.-J. Schmidt, A. Lohmann, and J. Richter, Eighth-order high-temperature expansion for general Heisenberg Hamiltonians, *Phys. Rev. B* **84**, 104443 (2011).
- [51] A. Lohmann, H.-J. Schmidt, and J. Richter, Tenth-order high-temperature expansion for the susceptibility and the specific heat of spin- $s$  Heisenberg models with arbitrary exchange patterns: Application to pyrochlore and kagome magnets, *Phys. Rev. B* **89**, 014415 (2014).
- [52] S. Yan, D. A. Huse, and S. R. White, Spin-Liquid Ground State of the  $s = 1/2$  Kagome Heisenberg Antiferromagnet, *Science* **332**, 1173 (2011).
- [53] S. Depenbrock, I. P. McCulloch, and U. Schollwöck, Nature of the spin-liquid ground state of the  $s = 1/2$  Heisenberg model on the kagome lattice, *Phys. Rev. Lett.* **109**, 067201 (2012).
- [54] A. M. Läuchli, J. Sudan, and R. Moessner,  $s = \frac{1}{2}$  kagome Heisenberg antiferromagnet revisited, *Phys. Rev. B* **100**, 155142 (2019).
- [55] J. Richter, O. Derzhko, and J. Schnack, Thermodynamics of the spin-half square kagome lattice antiferromagnet, *Phys. Rev. B* **105**, 144427 (2022).
- [56] R. Schäfer, I. Hagymási, R. Moessner, and D. J. Luitz, Pyrochlore  $S = \frac{1}{2}$  Heisenberg antiferromagnet at finite temperature, *Phys. Rev. B* **102**, 054408 (2020).
- [57] Y. Huang, K. Chen, Y. Deng, N. Prokof'ev, and B. Svistunov, Spin-Ice State of the Quantum Heisenberg Antiferromagnet on the Pyrochlore Lattice, *Phys. Rev. Lett.* **116**, 177203 (2016).
- [58] X. Chen, S.-J. Ran, T. Liu, C. Peng, Y.-Z. Huang, and G. Su, Thermodynamics of spin-1/2 kagome Heisenberg antiferromagnet: algebraic paramagnetic liquid and finite-temperature phase diagram, *Science Bulletin* **63**, 1545 (2018).
- [59] O. Derzhko, J. Richter, A. Honecker, and H.-J. Schmidt, Universal properties of highly frustrated quantum magnets in strong magnetic fields, *Low Temp. Phys.* **33**, 745 (2007).
- [60] O. Derzhko, J. Richter, and M. Maksymenko, Strongly correlated flat-band systems: The route from Heisenberg spins to Hubbard electrons, *Int. J. Mod. Phys. B* **29**, 1530007 (2015).
- [61] J. Schulenburg, *spinpack 2.58*, Magdeburg University (2019).
- [62] J. Richter and J. Schulenburg, The spin-1/2  $J_1 - J_2$  Heisenberg antiferromagnet on the square lattice: Exact diagonalization for  $N = 40$  spins, *Eur. Phys. J. B* **73**, 117 (2010).